Reprinted without change of pagination from
The Journal of Chemical Physics, Vol. 39, No. 12, December 15, 1963

(NASA Contract NAS7-100)
(JPL-TR-32-494)

Technical Report No. 32-494

Reaction between Nitric Oxide and Ozone in a Supersonic Nozzle

J. E. Marte,
E. Tschuikow-Roux, and
H. W. Ford

This paper presents results of one phase of research carried out at the Jet Propulsion Laboratory, California Institute of Technology, under Contract No. NAS 7-100, sponsored by the National Aeronautics and Space Administration.

JET PROPULSION LABORATORY
CALIFORNIA INSTITUTE OF TECHNOLOGY
PASADENA, CALIFORNIA

December 15, 1963

Reprinted from THE JOURNAL OF CHEMICAL PHYSICS, Vol. 39, No. 12, 3277–3285, 15 December 1963
Printed in U. S. A.

Reaction between Nitric Oxide and Ozone in a Supersonic Nozzle

J. E. MARTE, E. TSCHUIKOW-ROUX, AND H. W. FORD
Jet Propulsion Laboratory, California Institute of Technology, Pasadena, California

(Received 22 July 1963)

The rate of reaction between nitric oxide and ozone in a supersonic nozzle was measured in the temperature range 245–345°K by following the absorption of ultraviolet radiation by ozone at 2537 Å. The specific rate constant was found to be

$$k = 1.19 \times 10^{12} e^{-2500/RT} \text{ cm}^3 \cdot \text{mole}^{-1} \cdot \text{sec}^{-1}$$

The result is in good agreement with previous studies and confirms the bimolecular nature of the reaction. The experimental pre-exponential factor is in satisfactory agreement with one calculated from transition state theory.

INTRODUCTION

OZONE and nitric oxide are components of both the upper and the lower atmosphere. An accurate knowledge of their rate of reaction is one essential for a quantitative description of atmospheric reactions. Several previous investigations were limited in scope. The first such study is that of Johnston and Crosby,[1] who measured the rate at two temperatures and established the elementary bimolecular nature of the reaction

$$NO + O_3 \rightarrow NO_2 + O_2. \quad (1)$$

Subsequent investigators[2–4] measured the rate at a single temperature only.

The reaction appeared suitable for an extension of the supersonic nozzle technique developed by Wegener[5] for unimolecular decomposition. This method offered the advantage of quasisteady-state measurements and an extension of the temperature range. Experimental difficulties limited the advantages of the method, but good agreement with the earlier work was obtained over a wider temperature range than any previously covered by a single investigation.

The supersonic nozzle technique can be used in rate studies of any fast reaction in which one reactant will absorb light at a specific frequency.

EXPERIMENTAL

Description of Wind Tunnel

The wind tunnel used was especially designed for the purpose of studying reaction kinetics. A schematic diagram of the wind tunnel and associated equipment is shown in Fig. 1.

Nitrogen, stored in a large cascade at 2200 psi, was reduced in pressure and heated electrically, prior to reaching the nozzle inlet, to a supply temperature of about 400°K. The wedge-type supersonic nozzle design shown in Fig. 2 (diverging plane surfaces) of constant 3.20-cm width was designed to provide one-dimensional

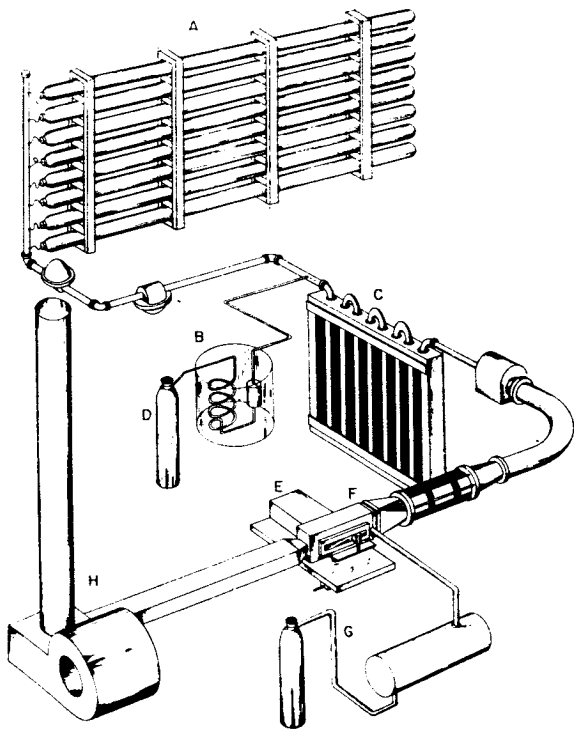

FIG. 1. Wind tunnel and associated equipment. A, N_2 cascade; B, flowmeter in ice bath; C, heater; D, NO supply; E, movable monochromator; F, nozzle section; G, ozonator and O_2 supply; H, blower and exhaust pipe.

flow with uniformly increasing Mach number, and calibration shows this to be closely approximated. The nozzle exit height was 2.00 cm and its throat height varied with Mach number. The over-all length was 15.00 cm, throat to exit, but only the 12.5 cm downstream from the throat were traversed. This type of

[1] H. S. Johnston and H. J. Crosby, J. Chem. Phys. **22**, 689 (1954).
[2] H. W. Ford, G. J. Doyle, and N. Endow, J. Chem. Phys. **26**, 1337 (1957).
[3] M. T. Borok, Russ. J. Phys. Chem. **35**, 1123 (1960).
[4] L. F. Phillips and H. I. Schiff, J. Chem. Phys. **36**, 1509 (1962).
[5] P. P. Wegener, Phys. Fluids **2**, 264 (1959).

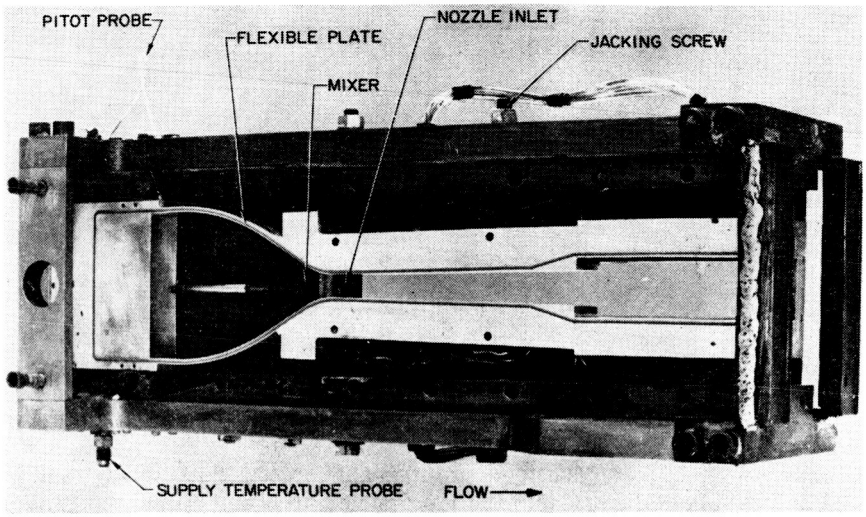

FIG. 2. Wind tunnel nozzle section.

nozzle differs from the contoured supersonic nozzle commonly used to obtain uniform flow in the test section, but has the advantage that a single set of nozzle blocks may serve for a range of exit Mach numbers. The presence of nonuniformities in the test section located downstream of the nozzle exit, a consequence of the wedge nozzle design, did not affect measurements made in the nozzle. The nozzle blocks were pinned near their ends to jacking screws, in a manner which permitted limited translation and rotation of the blocks in the vertical plane, thus allowing for variation of the nozzle throat height. The nozzle throat section was especially contoured to avoid the introduction of aerodynamic disturbances into the flow, at the junction of the curved throat portion of the nozzle and the plane supersonic part. Rectangular pieces of fused silica $\frac{1}{8}$ in. thick, mounted in molded silicone–rubber gaskets and supported by Micarta frames, were used as the nozzle side walls. The flow was expanded to atmospheric pressure in the exhaust by means of a 6° rectangular diffuser mounted to the nozzle exit.

After it passed through a flowmeter maintained at constant temperature (0°C), nitric oxide was introduced into the main stream by means of an orifice located immediately upstream of the heater. From this point to the nozzle, the pipe length was sufficient to ensure complete mixing with the nitrogen carrier gas. The ozone was injected into the main stream via a diffuser located 1 cm upstream of the nozzle throat.

Wall static orifices of $\frac{1}{32}$ in. diameter, located on the lower nozzle-block center line at 1-cm intervals over the throat and supersonic parts of the nozzle, were read by means of multiposition pressure switches on a single pot-type mercury manometer to measure static pressures. Stagnation pressure was measured with a pitot probe near the upstream edge of the upper flexible plate and read on a mercury-filled U-tube manometer.

The tunnel supply temperature was measured with a Chromel–Alumel total temperature probe, located at the station of the pitot probe on the lower flex-plate, and continuously recorded on a strip-chart recorder.

Spectrophotometer

The ultraviolet absorption of ozone at 2537 Å was measured photometrically as a function of position in the nozzle. A Pen Ray low-pressure mercury arc with associated power supply and isolation transformer was used as a light source for the photometer, because of its concentration of radiant energy at 2537 Å, and its stable operating characteristics. A diffraction grating monochromater, having a spectral slitwidth of 10 Å, isolated the 2537-Å line. The light beam emerging from the monochromator was collimated, and passed through the nozzle perpendicular to the flow onto an RCA 7200 photomultiplier tube detector through a shield which was in the form of a 1.4×10 mm vertical slit located 1.5 in. from the photocathode. The detector output was fed into one input of an X–Y recorder. During early experiments a beamsplitter, located between the monochrometer exit and the tunnel window, was used to deflect a portion of the light beam into a second matching photomultiplier, the output of which was monitored on a second X–Y plotter to determine the fluctuations in light intensity during an experimental run. This proved to be unnecessary and was discontinued.

The entire photometer was rigidly mounted to a horizontal carriage located beneath the nozzle section of the wind tunnel. This table was driven in a direction parallel to the nozzle center line by means of a motor-operated lead screw. This arrangement permitted measurement of light transmission over a 12.5-cm region downstream from the nozzle throat. A position-indicating potentiometer mounted to the table base and a wiper mounted to the moving table provided a

position signal, which was used as a second input to the X–Y recorder, thus providing a continuous plot of light intensity versus nozzle position. The accuracy of the position indication was 0.5 mm.

Ozone Mixer

The distribution of ozone in the flowing mixture of nitrogen and nitric oxide proved to be an important experimental difficulty because of conflicting requirements arising, on the one hand, from limitation on ozone concentration at the nozzle-injection point, and on the other from gas dynamic problems of nozzle blockage and mixing length. Experiments showed that diffusive mixing was negligible in the short residence times possible between the point of injection and the most upstream point of observation. This required that the ozone be transported within the mixer in such a manner that distribution be essentially uniform when injected into the main flow. Because the reaction under study is first order with respect to ozone concentration, the determination of the specific rate constant by absorption measurement is independent of ozone concentration along the light beam, i.e., in a horizontal line perpendicular to the direction of flow. Therefore, it is only necessary that the mixer distribute the ozone uniformly in the vertical plane. This fact led to a mixer in the form of a two-dimensional diffuser mounted with the exit, a narrow vertical slit, facing downstream on the vertical centerline of the tunnel and essentially spanning the tunnel vertically as shown in Fig. 2.

A series of light-intensity ratio profiles made at various fixed nozzle stations, with ozone present in supersonic flow, were made by traversing the photometer vertically, and showed the vertical distribution to be approximately uniform throughout the nozzle. For this work, the slit mask on the photomultiplier was replaced by an orifice of dimensions 0.8×0.8 mm.

Reactants

The ozone was produced in a voltage-regulated Welsbach model C-4 ozonator supplied with technical grade oxygen at the rate of 3.4×10^4 cm³/min STP, and produced a continuous flow of ozone of about 170 cm³/min at the tunnel end of the supply line. The use of an anhydrous magnesium perchlorate drying trap produced no discernible increase in ozone output and was eliminated after testing. Although it was necessary to operate the ozonator at an inefficiently high pressure of 20–30 psig, in order to maintain a mixer outlet pressure high enough to produce a usable rate of flow into the tunnel, the rate of production of ozone was sufficiently constant to permit the ozonator output to feed directly into the mixer during an experiment. Ozone concentrations of the order of 10^{-9} moles per cm³ were measured in the nozzle.

Matheson nitric oxide of 99% stated purity was used directly from the supply tank without further purification. Oil-free nitrogen from the high-pressure supply cascade was used as the carrier gas. The supply pressure was 2 atm, which resulted in nitrogen concentration in the nozzle of the order of 10^{-5} moles/cm³.

DISCUSSION

Determination of the Rate Constant

The rate of change of ozone concentration in a flow system, such as a supersonic nozzle due to chemical reaction, may be determined as the difference between the rate of change of concentration with reaction present and the rate of change of concentration with the reaction frozen, i.e.,

$$d(O_3)/dt=[d(O_3)/dt]_{obs}-[d(O_3)/dt]_F. \quad (2)$$

Furthermore, in a steady supersonic flow, a quasi-steady-state condition with regard to the reaction can be maintained. Hence, at any fixed position in the nozzle, the ozone concentration is invariant with time,

$$[d(O_3)/dt]_x=0. \quad (3)$$

For one-dimensional steady flow, $[d(O_3)/dt]_{obs}$ is given by

$$\left[\frac{d(O_3)}{dt}\right]_{obs}=\left[(O_3)\frac{\partial u}{\partial x}+u\frac{\partial(O_3)}{\partial x}\right]_{obs}+D\left[\frac{\partial^2(O_3)}{\partial x^2}+\frac{\partial^2(O_3)}{\partial y^2}\right]_{obs}+\frac{\partial(O_3)}{\partial t}, \quad (4)$$

where u is the flow velocity, D the diffusion coefficient, x the axis along the nozzle centerline and y the vertical axis. The terms on the rhs of Eq. (4) represent, respectively, the flux of (O_3) due to convection, diffusion, and chemical reaction. As discussed earlier, the diffusion along the third axis, if any, has no effect on the chemical rate. Furthermore, numerical evaluation of the diffusion terms and the acceleration term shows them to be negligible; thus Eq. (4) reduces to

$$\left[\frac{d(O_3)}{dt}\right]_{obs}=u\left[\frac{\partial(O_3)}{\partial x}\right]_{obs}+\frac{\partial(O_3)}{\partial t}. \quad (5)$$

Since the concentration of nitric oxide was greater by two orders of magnitude than that of ozone, the rate of disappearance of ozone (due to the reaction) determines the rate of the reaction

$$-[\partial(O_3)/\partial t]=k(O_3)(NO). \quad (6)$$

From Eqs. (5) and (6) we obtain

$$[d(O_3)/dt]_{obs}=u[\partial(O_3)/\partial x]_{obs}-k(O_3)(NO). \quad (7)$$

Similar considerations lead to

$$[d(O_3)/dt]_F=u[\partial(O_3)/\partial x]_F \quad (8)$$

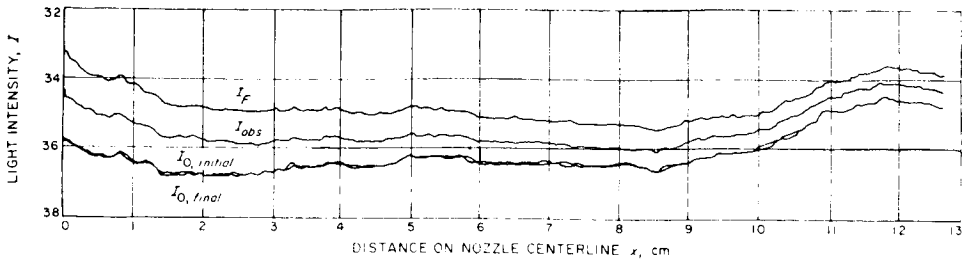

FIG. 3. Raw data trace.

for the frozen reaction. The low concentration of ozone (0.1%) relative to the carrier permitted the flow properties, such as velocity, to be considered as unaffected by the heat of the reaction.

Substitution of Eqs. (7), (8), and (3) into Eq. (2) yields the expression for the specific rate constant at a fixed x position,

$$k=u\left\{\left[\frac{\partial(O_3)}{\partial x}\right]_{obs}-\left[\frac{\partial(O_3)}{\partial x}\right]_F\right\}\Big/[(O_3)(NO)]. \quad (9)$$

An example of the raw data of the photometer, from which the ozone concentration as a function of distance down the nozzle was calculated, is shown in Fig. 3. The $I_{0,\text{initial}}$ trace is the signal obtained from a traverse of the nozzle with side walls in place, but with only nitrogen flowing in the tunnel. The I_F trace was made with the ozone added to the nitrogen, as soon as the output of the ozonator reached an equilibrium value, a delay of several minutes. The I_{obs} trace was made by adding the nitric oxide to the ozone and nitrogen immediately following the I_F survey. The $I_{0,\text{final}}$ trace was then made to check for changes in light transmission during the run. A single traverse of the nozzle required about 10 seconds and the entire sequence, which constituted a run, required 3–4 min.

The relationship between the various I traces in Fig. 3 is somewhat obscured by the presence of a film on the inner surfaces of the side walls, which made the transmission through the windows a function of position. This film built up on the clean windows prior to measurement of the first I trace, and remained approximately constant thereafter as the good agreement between the I_0 traces indicate. The I_{obs} and I_F traces were also reproducible over the time period of a run. In Fig. 4, the data from Fig. 3 has been read at $\frac{1}{2}$-cm intervals and plotted as the ratio of I_{obs}/I_0 and I_F/I_0. Smooth curves were then faired through the data points, and readings from the curves were used to obtain ozone concentrations utilizing the Beer–Lambert law

$$\log I/I_0=-\epsilon W(O_3), \quad (10)$$

where ϵ is the molar extinction coefficient and W the nozzle width. Recently Hearn[6] reported the absorption coefficient $\alpha=133.9$ cm^{-1} for O_3 at 0°C and 1 atm, from which can be obtained the molar extinction coefficient $\epsilon=\alpha M_{O_3}/\rho_{O_3}=3.001\times10^6$ cm^2/mole where M_{O_3} is the molecular weight of O_3 and ρ_{O_3} is density of O_3 at the pressure and temperature of ϵ. The ozone concentration obtained in this manner is $(O_3)=-1.042\times10^{-7}\log(I/I_0)$ when 3.2 cm is used for W. From this equation, $(O_3)_{obs}$ and $(O_3)_F$ can now be obtained from I/I_0 curves as functions of nozzle position, x.

The differential terms in Eq. (9), $[\partial(O_3)/\partial x]_F$ and $[\partial(O_3)/\partial x]_{obs}$ were obtained by measurement of the slopes of faired curves through the experimental values

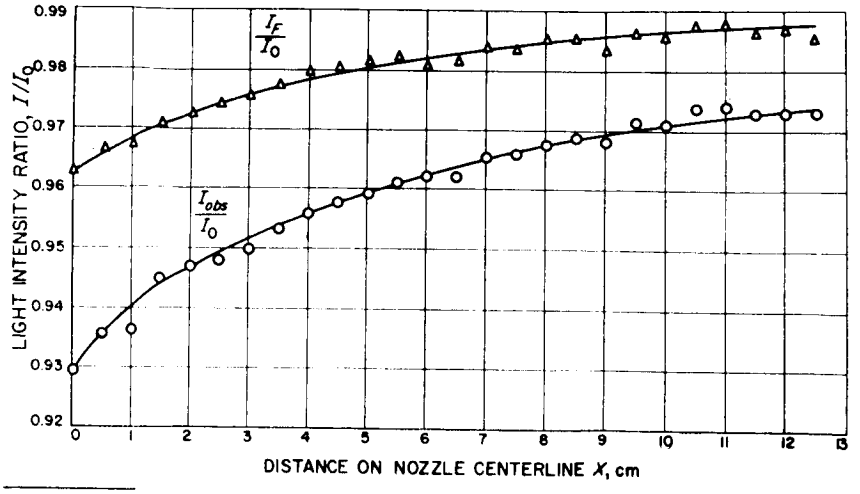

FIG. 4. Light intensity ratios in nozzle.

[6] A. G. Hearn, Proc. Phys. Soc. (London) 78, 932 (1961).

of $(O_3)_F$ and $(O_3)_{obs}$, using the approximation that $\Delta(O_3)/\Delta x=\partial(O_3)/\partial x$ where $\Delta x=1$ cm.

For low concentrations of nitric oxide in the carrier gas, the equation of continuity at the nozzle sonic throat may be written, for convenience, in the form

$$dm_{NO}/dt=(a_*/a_0)(\rho/\rho_0)a_0(NO)M_{NO}A_*, \quad (11)$$

where $a=(\gamma RT)^{\frac{1}{2}}$ is the velocity of sound, ρ the flow density, and A_* is the nozzle throat cross-section area. The subscripts 0 and * refer to stagnation and nozzle throat conditions, respectively. For a given ratio of specific heats, γ; (a_*/a_0) and (ρ_*/ρ_0) are constant and known from gas dynamic considerations. In the present calculations the value $\gamma=1.40$, corresponding to pure nitrogen, was used since the contribution of nitric oxide and ozone is negligible in this respect. The mass-flow term on the left side of Eq. (11) was obtained from a calibrated flowmeter reading, as the rate at which nitric oxide was added to the carrier gas. The mass flow of nitric oxide was such that $(NO)=100\times(O_3)$, i.e., $(NO)_0=10^{-7}$ moles/cm^3, and thus was considered unaffected by the reaction. Furthermore, since mixing between NO and N_2 carrier was taken as complete, $(NO)=(\rho/\rho_0)(NO)_0$, where (ρ/ρ_0) is a function of position in the nozzle. Substituting this in Eq. (11),

$$(NO)=\frac{(\rho/\rho_0)(dm_{NO}/dt)}{(a_*/a_0)(\rho_*/\rho_0)a_0M_{NO}A_*} \quad (12)$$

is obtained.

The remaining term needed to solve Eq. (9) for the rate constant is u, the flow velocity, given in terms of the Mach number, M, and the sound velocity, a, by $u=Ma=M[\gamma R(T/T_0)T_0]^{\frac{1}{2}}$ where (T/T_0) is a well-known and tabulated function of the Mach number. M was determined by calibration of the nozzle and T_0 is a measured value.

As with any measurement of this type in a flow system, the effect of the side-wall boundary layers must be considered. In the turbulent boundary layers found in this nozzle, the wall temperature was approximately equal to the supply temperature T_0, which was higher than the ambient temperature of the main flow. Thus, there existed a temperature gradient across the boundary layer. Additionally, flow velocity in the boundary layer varied from the free stream value at the outer edge to zero at the wall, which resulted in longer residence times near the wall. Further, the thickness of the boundary layer varied from essentially zero at the nozzle throat to 17% of the optical path length at the exit. A calculation of the upper limit on the boundary layer effect, Appendix A, gives an increase in k of 8%. The experimental accuracy is insufficient to warrant the use of this correction, so all absorption data are reduced according to Eq. (9).

The logarithms of the specific rate constants obtained in this manner are plotted against $10^3/T$ in Fig. 5. A least-squares straight line has been drawn through the 80 experimental points. Writing the rate constant for Reaction (1) in the Arrhenius form, $k=A\exp(-E/RT)$, the values of E and A obtained from Fig. (5) are, respectively, $E=2.55\pm0.22$ kcal/mole, and $A=1.19\times10^{12}$ cm^3·mole^{-1}·sec^{-1}. The result is in good agreement with the work of Johnston and Crosby, who reported $E=2.5\pm0.3$ kcal/mole and $A=0.8\times10^{12}$ cm^3·mole^{-1}·sec^{-1}.

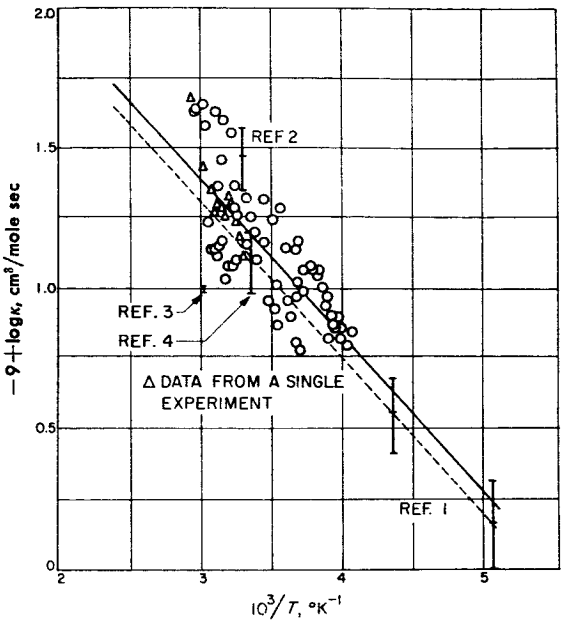

FIG. 5. Temperature dependence of rate constants.

Their data, along with other measurements of the reaction[2-5] are included in the figure for comparison. The vertical bars represent scatter of these data. The relatively good agreement between all the data is interesting in view of the wide variety of experimental techniques applied in obtaining the data. Johnston and Crosby used a constant cross-section-area subsonic flow system and an ultraviolet photometer to measure ozone concentration. Phillips and Schiff and Borok also used low-velocity flow systems of constant cross-section area but the former utilized a mass spectrometer to measure both ozone and nitric oxide concentration, while the latter introduced known amounts of nitric oxide under conditions which assured full oxidation. In addition, Borok checked his work by means of an automatic photocalorimetric analyzer. Ford, Doyle, and Endow, using a stirred flow reactor and trace reactant concentrations, photolyzed nitrogen dioxide in the presence and absence of added ozone and analyzed for ozone with an ultraviolet photometer.

Most of the scatter in the present data appears to be a result of the form of differential terms $[\partial(O_3)/\partial x]_F$ and $[\partial(O_3)/\partial x]_{obs}$ in Eq. (9). These must be evaluated as the slopes of fairings of the experimental measurements of ozone concentration plotted versus position

in the nozzle. Integration of Eq. (9) leads to an equivalent problem.

The use of an ozonator of moderate size together with the mass-flow requirement of the nozzle, necessitated the low concentration of ozone in the flow system. As Fig. 4 indicates, the change in absorbtion due to the reaction was as little as 1.5% in the downstream portions of the nozzle. In order to obtain useful measurements of ozone concentrations in this absorption range, it was necessary that sources of scatter in the data such as light-intensity fluctuation and drift as well as variation in the ozone supply and distribution, be kept to a minimum. The fluctuation of light intensity including noise in the photomultiplier and X–Y recorder was measured as 0.15% of the full scale value. Only runs in which the drift and window film buildup were negligible were used as data. The small amount of variation in the ozone supply under equilibrium conditions was indicated by the facts that the I_F trace was repeatable over the time required for a complete run, and that the small-scale fluctuations in the I_F trace were of the same order of magnitude as those in the I_0 traces. Over-all scatter of the raw data as determined from I/I_0 ratios, as shown in Fig. 4, is $\pm 0.2\%$. The accuracy of movements in the x position of the absorption beam was known to about ± 0.5 mm.

The considerable temperature range of the present data is worth noting, for it illustrates one of the principal advantages of the supersonic nozzle as a tool for the measurement of fast reaction rates. The data of the present experiments were obtained in eleven experiments ranging in nozzle-exit Mach number from 1.14 to 1.74 and in temperature from 245° to 345°K. The data points marked with the symbol (Δ) are a single experiment and serve to illustrate the temperature range and variation of the data during one experimental run.

Calculation of Rate Constant from Transition-State Theory

It is of some interest to compare the experimental pre-exponential factor (A_{exptl}) with one calculated, for example, from transition-state theory. In view of the close agreement between the values of A_{exptl} found here and those of previous investigators, the experimental value appears to be well established. Thus a theoretical calculation may provide a test of the consistency of the theory, or more precisely, of the activated complex itself and the various assumptions associated with it. A crude calculation of this type has been made by Herschbach *et al.*,[7] and a somewhat more refined one will be given here.

The calculated pre-exponential factor, A_{theor}, commensurate with A_{exptl} is given by

$$\ln A_{\text{theor}} = \ln B(T) + [T d \ln B(T)/dT], \qquad (13)$$

where $B(T)$ is proportional to the partition function ratio of the activated complex to reactants, and occurs in the theoretical rate expression

$$k_{\text{theor}} = B(T) \exp(-V/RT), \qquad (14)$$

where V is temperature independent. If the partition functions are expressed in terms of local properties of the molecules,[8–10] then for Reaction (1), $B(T)$ is given by

$$B(T) = \kappa\left(\frac{\sigma_A\sigma_B}{\sigma_\ddagger}\right)\left(\frac{Q_{\text{el}}{}^\ddagger}{Q_{\text{el}}{}^A Q_{\text{el}}{}^B}\right)\frac{\prod_2^5 \mathcal{J}_\alpha{}^\ddagger}{\mathcal{J}_2{}^A \prod_2^3 \mathcal{J}_\alpha{}^B} \times \frac{\prod_1^6 \Gamma_i{}^\ddagger}{\Gamma_1{}^A \prod_1^3 \Gamma_i{}^B} \frac{\prod_2^7 \ell_i{}^\ddagger}{\ell_1{}^A \prod_1^3 \ell_i{}^B} (\ell_{\text{IR}}{}^\ddagger)^2 \nu^* w^{-1}, \qquad (15)$$

where as usual κ denotes the transmission coefficient, which here is assumed to be unity, σ the symmetry number, and Q_{el} the electronic partition function. The $\mathcal{J}$'s are the Jacobian (geometrical) factors; $\ell_i = (2\pi kT/f_{ii})^{\frac{1}{2}}$ is a vibrational amplitude factor associated with the diagonal force constant f_{ii}, and $\ell_{\text{IR}}{}^\ddagger$ is a similar amplitude factor for internal rotation. In the present treatment we have assumed free internal rotation in which case the amplitude factor is simply given by $\ell_{\text{IR}} = 2\pi$. The factor $w = [1 - (f_{23}{}^2/f_{22}f_{33})]^{\frac{1}{2}}$ is an imaginary quantity which corrects for the off-diagonal interaction force constant associated with the "reaction coordinate"; ν^* is the imaginary frequency along this reaction coordinate; and $\Gamma_i = (u_i/2)/\sinh(u_i/2)$ is a quantum correction factor, where $u_i = h\nu_i/kT$. The indices ‡, A, and B refer to activated complex, NO, and O_3, respectively. The $\mathcal{J}$ factors depend on the geometry of the reactants and the activated complex and are listed in Table I. A list of the $\mathcal{J}$ factors for various geometric configurations and a method to evaluate them is given in Ref. 8. A force constant assignment must be made to evaluate the ℓ_i factors. To evaluate the Γ_i factors a vibrational analysis of the activated complex is necessary.

[7] D. R. Herschbach, H. S. Johnston, K. S. Pitzer, and R. E. Powell, J. Chem. Phys. **25**, 736 (1956).

[8] D. R. Herschbach, H. S. Johnston, and D. Rapp, J. Chem. Phys. **31**, 1652 (1959).

[9] H. S. Johnston, Advan. Chem. Phys. **3**, 131 (1960).

[10] H. S. Johnston and D. Rapp, J. Am. Chem. Soc. **83**, 1 (1961).

TABLE I. Geometrical and force parameters for reactants, activated complex, and reaction products.

	NO	O_3	$ON-O_3$ Complex[f]	NO_2	O_2
σ	1	2	1	2	2
Q_{el}	$2+2\exp(-121.1/kT)$	1	2	2	3
$R\times10^8$ cm	1.1508[b]	1.26[c,d]	1.169(R_1) 1.402(R_2) 1.474(R_3) 1.234(R_4)	1.188[e]	1.2074[b]
Bond angle	...	127°[c,d]	130° (all ∢)	134°[e]	...
$\prod_{\alpha=2}^{N} \mathfrak{I}_\alpha$	$4\pi R_A^2$	$8\pi^2 R_B^4 \sin\phi_B$	$8\pi^2 R_1^2 R_2^2 R_3^2 R_4^2 \sin^3\phi_\ddagger$	...	...
$f_{stretch}\times10^{-5}$ (dyn/cm)	15.943[b]	4.643[c,d]	f_{11} 13.616 f_{22} 5.644 f_{33} 2.322 f_{44} 8.204 f_{23} 3.6198	11.288[a]	11.765[b]
$f_{bend}\times10^{11}$ (ergs/radian²)	...	2.693[c,d]	f_{55}(ONO) 1.666 f_{66}(NOO) 1.752 f_{77}(OOO) 2.693	1.666[a]	...

[a] Calculated from data of Ref. e assuming a valence force field.
[b] G. Herzberg, *Infrared and Raman Spectra* (D. Van Nostrand, Inc., Princeton, New Jersey, 1959).
[c] M. J. Klein, F. F. Cleveland, and A. G. Meister, J. Chem. Phys. **19**, 1068 (1951).
[d] W. Shand, Jr., and R. A. Spurr, J. Am. Chem. Soc. **65**, 179 (1943).
[e] G. E. Moore, J. Opt. Soc. Am. **43**, 1045 (1953).
[f] For calculational purposes, the parameters for the activated complex are listed to four figures. However, due to the assumptions involved in obtaining these quantities, their accuracy is at best two figures.

The planar model chosen for the activated complex is given in Fig. 6. The linkages between atoms are dictated by the products formed.[7] Since the activated complex is, by microscopic reversibility, an intermediate between reactants and products, the geometric parameters were chosen accordingly. Thus the bond distances for end atoms were taken as averages of the bond distances in NO and NO_2, and O_3 and O_2, respectively. The bond distances of the two middle bonds were calculated, respectively, from the bond distances in NO_2 and O_3 using Pauling's rule[11] for bond order and bond distances and assuming the bond order to be one-half that of the stable molecule, i.e.,

$$R(n/2)=R(n)+0.71\log 2.$$

All bond angles were taken to be 130°, a value intermediate between the bond angles in NO_2 and O_3.

The stretching-force constants for the end bonds were taken as averages of the NO and NO_2, and the O_3 and O_2 stretching-force constants, respectively. The stretching-force constants for the middle bonds were calculated for one-half-order bonds from the simple empirical formula,[9] $f(n/2)=\frac{1}{2}f(n)$. The bending force constants for end bonds should not differ significantly from the bending-force constants found in products and reactants.[7] The force constant for the bending around the central atom is much more difficult to estimate and a $3N-6$-dimensional potential energy hypersurface would be required, in principle, to obtain this force constant in analogy to Eyring's three-dimensional semiempirical method[12] for linear triatomic complexes. Such a surface is, of course, difficult to visualize. We,

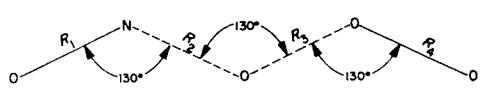

FIG. 6. Planar model of $ON-O_3$ complex.

[11] L. Pauling, *The Nature of the Chemical Bond* (Cornell University Press, Ithaca, New York, 1960).

[12] S. Glasstone, K. J. Laidler, and H. Eyring, *The Theory of Rate Processes* (McGraw-Hill Book Company, Inc., New York, 1941).

TABLE II. Vibrational frequencies of NO, O_3, and ON–O_3 complex.[a]

NO	O_3	ON–O_3
		$A_{max}=0.680\times10^{12}$ cm^3·mole^{-1}·sec^{-1}
		$f_{23}=3.62\times10^5$ dyn/cm
1904.0	1322.5(ν_1)	1834 sym. str. of ends
	750.9(ν_2)	1368 sym. str. of middle
	1616.0(ν_3)	1227 antisym. str. of ends
		845 antisym. bend of ends
		722 sym. bend of ends
		304 sym. bend of middle
		~0 antisym. str. of middle

[a] All frequencies in cm^{-1}.

therefore, again take this force constant, *a priori*, to be equal to one-half the bending force constant in ozone.[9] The various geometric and force parameters for the reactants and activated complex are summarized in Table I.

With the above parameters assigned, one has still to specify the interaction force constant f_{23} associated with the reaction coordinate in order to evaluate w^{-1} and the Γ_i factors needed in Eq. (15). At present there is no rigorous method to assess this force constant for a nonlinear activated complex. We shall, therefore, resort to a method outlined by Johnston and coworkers[7,9] and choose its value to make a flat-topped barrier, i.e., we choose f_{23} to make the imaginary frequency in the reaction coordinate virtually zero. With the f_{23} value thus specified, the vibrational frequencies have been calculated using Wilson's FG-matrix method[13] by means of an IBM–7094 computer and are listed in Table II. The pre-exponential factor was then evaluated from Eqs. (13) and (15) at 300°K and found to be: $A=0.757\times10^{12}$ cm^3·mole^{-1}·sec^1 compared to our experimental value of 1.19×10^{12} cm^3·mole^{-1}·sec^{-1}. The agreement must be ruled quite fortuitous considering the various assumptions used in the calculation, which is at best reasonable to a factor of 5 to 10.

ACKNOWLEDGMENTS

We wish to thank Professor S. Benson for his helpful discussion of this work. We thank the referee for his careful review and helpful advice.

APPENDIX A: CALCULATION OF THE EFFECT OF THE SIDE WALL BOUNDARY LAYER ON THE SPECIFIC RATE CONSTANT

Taking the thickness of one boundary layer as δ, the rhs of Eq. (10) can be separated into boundary-layer and free-stream terms. Equation (10) can therefore be written in the form

$$-\log\sigma=\epsilon(W-2\delta)(O_3)+2\delta\epsilon(O_3)_\delta, \quad \text{(A1)}$$

and hence

$$(O_3)=[-\log\sigma+2\delta\epsilon(O_3)_\delta]/[\epsilon(W-2\delta)], \quad \text{(A2)}$$

where (O_3) is free-stream concentration, $(O_3)_\delta$ is the average concentration in the boundary layer and $\sigma=I/I_0$. Differentiating Eq. (A2) with respect to the position coordinate x gives

$$\left[\frac{d(O_3)}{dx}\right]_{obs}=(W-2\delta)^{-2}\left\{[\epsilon^{-1}\log\sigma+2\delta(O_3)_\delta]\left(-\frac{2d\delta}{dx}\right)\right.$$

$$\left.+(W-2\delta)\left[\sigma^{-1}\frac{d(\log\sigma)}{dx}+\frac{2\delta d(O_3)_\delta}{dx}+2(O_3)_\delta\frac{d\delta}{dx}\right]\right\}. \quad \text{(A3)}$$

No method was available to measure $(O_3)_\delta$, and since the multiplicity of variables makes a computation of ozone concentration in the boundary layer of doubtful accuracy, it becomes necessary to make the limiting assumptions that $(O_3)_\delta$ and $d(O_3)_\delta/dx$ are equal to zero in the case with chemical reaction present. Equation (A3) then reduces to

$$\left[\frac{d(O_3)}{dx}\right]_{obs}=-\left[\frac{2\log\sigma}{\epsilon(W-2\delta)^2}\frac{d\delta}{dx}+\frac{1}{\epsilon(W-2\delta)}\frac{d(\log\sigma)}{dx}\right]. \quad \text{(A4)}$$

Using measurements from a particular experiment, Eq. (A4) can be evaluated. From measurements of boundary-layer displacement thickness, the boundary-layer thickness at the nozzle exit ($x=15$ cm) is calculated to be $\delta=0.28$ cm. Taking the boundary-layer thickness to be a linear function of the distance from the nozzle throat and originating at the throat, the expression for $\delta=f(x)$ is $\delta=0.28(x/15)$, where x and δ are in centimeters. In addition the derivative of δ with respect to x is $d\delta/dx=0.28/15=0.019$ and the nozzle width $W=3.2$ cm. The molar extinction coefficient has been given as $\epsilon=3.001\times10^6$ cm^3/mole and the remaining terms in Eq. (A4) are obtained from experimental data taken at the point of measurement furthest downstream in the nozzle; i.e., the point at which the boundary layer thickness is greatest. The necessary numerical values thus obtained are

$$\delta=0.28(11.5/15)=0.215 \text{ cm},$$

$$\log\sigma=-0.00709,$$

$$d(\log\sigma)/dx=0.00040.$$

Substituting these values into Eq. (A4),

$$[d(O_3)/dx]_{obs}=-0.0364\times10^{-9} \text{ mole/cm}^4$$

is obtained. The comparable value without the boundary-layer connection is -0.0420×10^{-9} mole/cm^4. Because of the form of Eq. (4), it is clear that the effect on the specific rate constant is greatest when the difference between the differential terms in the numerator is at a maximum. This occurs when $(O_3)_\delta=(O_3)$ for the frozen case; i.e., when the assumption is

[13] E. B. Wilson, Jr., J. C. Decius, and P. C. Cross, *Molecular Vibrations* (McGraw-Hill Book Company, Inc., New York, 1955).

made that there is no change in the ozone concentration between free stream and boundary layer. This leads directly to the result that $[d(O_3)/dx]_F$ is not changed from its uncorrected value.

To evaluate the corrected ozone-concentration term appearing in Eq. (4), the assumption that $(O_3)_s=0$ in the reaction case is applied in Eq. (A2) which reduces to

$$(O_3) = -\log\sigma/[\epsilon(W-2\delta)], \qquad (A5)$$

from whence $(O_3)=0.853\times10^{-9}$ mole/cm^3.

Substitution into Eq. (4) of the corrected terms along with appropriate values for u and (NO), which are unaffected by the correction, results in the specific rate constant as corrected for the boundary-layer effect, $k=1.40\times10^{10}$ cm^3/mole·sec. The uncorrected value for k at the same location is 1.29×10^{10} cm^3/mole·sec. This represents a correction of 8.5% in the upper limit since the boundary layer is thinner at all other usable locations and, in addition, the limiting assumptions on $(O_3)_s$ and its derivative may not be fully realized.